Journal of Power Sources 222 (2013) 518–525

Contents lists available at SciVerse ScienceDirect

Journal of Power Sources

journal homepage: www.elsevier.com/locate/jpowsour

A graphene-multi-walled carbon nanotube hybrid supported on fluorinated tin oxide as a counter electrode of dye-sensitized solar cells

Li-Hsueh Chang [a,1], Chien-Kuo Hsieh [b,c,1], Min-Chien Hsiao [a], Jen-Chi Chiang [a], Po-I. Liu [a], Kuan-Ku Ho [a], Chen-Chi M. Ma [a,*], Ming-Yu Yen [a], Ming-Chi Tsai [d], Chuen-Horng Tsai [d]

[a] Department of Chemical Engineering, National Tsing Hua University, Hsinchu 30013, Taiwan, ROC
[b] Department of Materials Engineering, Mingchi University of Technology, Taipei 24301, Taiwan, ROC
[c] Center for Thin Film Technologies and Applications, Mingchi University of Technology, Taipei 24301, Taiwan, ROC
[d] Department of Engineering and System Science, National Tsing Hua University, Hsinchu 30013, Taiwan, ROC

HIGHLIGHTS

- A hybrid material consisting of multi-walled carbon nanotubes and grapheme was used.
- The hybrid material provides a higher charge transfer rate and a lower internal resistance.
- Hybrid electrodes possesses higher rate of charge transfer and lower electron lifetime.
- Hybrid counter electrode cell performance reached 91.6% of platinized electrode.

GRAPHICAL ABSTRACT

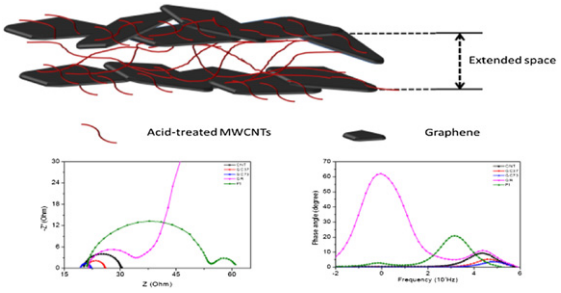

ARTICLE INFO

Article history:
Received 21 May 2012
Received in revised form
16 August 2012
Accepted 21 August 2012
Available online 10 September 2012

Keywords:
Graphene
Carbon nanotubes
Hybrid
Counter electrode
Dye-sensitized solar cells

ABSTRACT

We report a solution-based method to prepare a hybrid material consisting of multi-walled carbon nanotubes and graphene. Raman spectroscopy shows that a decrease in the concentration of defects of hybrid, compared to graphene, which is confirmed by the D/G ratio, implying the repair of the conjugation system. Due to the increased surface areas of graphene and the increased spaces between graphene sheets, results of cyclic voltammetry and electrochemical impedance spectroscopy show that the electrocatalytic ability of the hybrid material affords a higher charge transfer rate, an improved exchange current density, and a lower internal resistance. Transmission and scanning electron microscopy images show that the hybrid counter electrode has a rough and porous structure, resulting in a lower resistance to diffusion, thereby increasing the total redox reaction rate at the counter electrode. Hybrid electrodes have a number of advantages over other electrodes made of graphene or platinum films, including a higher rate of charge transfer, a lower internal resistance, a lower resistance to diffusion, and a lower electron lifetime. The cell performance using a hybrid counter electrode (4.66%) reached 91.6% of that of cells prepared using a platinized fluorinated tin oxide electrode (5.09%).

1. Introduction

Dye-sensitized solar cells (DSSCs) have considerable potential for the development of applications in “green” energy due to their low cost and high performance [1,2]. DSSC devices consist of transparent conductive glass (TCO), sensitized TiO_2 with dye,

* Corresponding author. Tel.: +886 35713058; fax: +886 35715408.
E-mail address: ccma@che.nthu.edu.tw (C.-C.M. Ma).
[1] Co-first authors with equal contribution.

0378-7753/$ – see front matter © 2012 Elsevier B.V. All rights reserved.
http://dx.doi.org/10.1016/j.jpowsour.2012.08.058

electrolyte, and platinized TCO. The principle of operation of DSSCs is the photo-induced oxidation of a dye molecule on a working TiO_2 electrode; in the process, the oxidized dye molecule is reduced by I^-. The oxidized species diffuses from the surface of the dye to the counter electrode and regenerates I^- with the assistance of a catalyst. Platinum is the catalyst conventionally used in a DSSC because it exhibits a strong electrocatalytic activity for the iodide/triiodide redox species. However, the poor stability and high cost of platinum means an alternative to it is required for the further development of the counter electrode of DSSCs.

The potential of various carbonaceous materials has been demonstrated in the search for alternative catalysts to platinum; these include carbon black [3–5], carbon nanotubes [6–11], and graphite [12,13]. The recent use of the two-dimensional carbon-based material graphene (GR) has shown it to be the most attractive alternative to platinum, due to its high electrical conductivity and high specific surface area [14–18]. Several authors have demonstrated the variable charge transfer resistance and the electrochemical properties of GR [14–18]. Defect-rich GR has been shown to be a favored as an alternative material for use as a counter electrode, as a result of its high concentration of active sites and high specific surface area. However, due to its high aspect ratio, GR is inclined to aggregation, which inhibits its active defect area, thereby leading to an increased internal resistance and the increased diffusion resistance of the redox species [19]. Hence, several authors have demonstrated a novel method of enhancing the electrochemical behavior of GR by incorporating carbon nanotubes (CNTs) into its structure. Choi et al. demonstrated the use of a graphene-based MWCNT (GMWCNT) structure as a counter electrode catalyst through the use of chemical vapor deposition [18,20]. According to electrochemical impendent spectra and performance data, they suggested that GMWCNTs may be a promising material for the counter electrodes of DSSCs. Zhu et al. presented GR-CNTs films by using electrophoretic deposition (EPD) [21] and in so doing achieved a high efficiency of 6.17%. To develop the technology of DSSCs, however, more convenient method of preparing a counter electrode catalyst is required. In our previous study, we demonstrated the use of a carbonaceous hybrid material comprised of multi-walled carbon nanotubes (MWCNTs) and GR, and showed the unique properties of this material for enhancing the rate of charge transfer through the formation of a three dimensional conductive network [22]. In addition, it is possible to control the dispersion and microstructure of the GR through the ratio of GR to MWCNTs, thereby preventing the restacking of GR. Due to the increased spacing of the GR layers, the morphology of the GR may be manipulated through the incorporation of MWCNTs in order to increase the active surface area, thereby improving the electrochemical properties. Furthermore, the high internal resistance is a result of the conducting path of the GR and due to the hopping of the delocalized π-electrons. In the present study, we demonstrate a simple approach for preparing a hybrid carbonaceous material using a one-step solution-based method at room temperature, as shown in Fig. 1. To date, there have been no reports of a GR/MWCNT (GC) hybrid electrode on the fluorinated tin oxide (FTO) fabricated using a solution-based method.

2. Experimental

2.1. Preparation of graphene oxide (GO), GR, and GC hybrid materials

We prepared GO using the method described in our previous study [19]. 10 g of graphite flakes and 50 g potassium permanganate ($KMnO_4$) were stirred in a solution containing concentrated H_2SO_4 and HNO_3 for several days, and this solution was then reacted with H_2O_2 and washed with 5 wt% aqueous hydrochloric acid solution (HCl) to allow the oxidation to be completed and to remove the sulfate ions. The suspension was washed with deionized water and centrifuged repeatedly until the pH of the solution was neutral. Finally, the resulting brown powder was dried in a vacuum at room temperature to obtain GO. The GC hybrid was obtained by means of a chemical reduction using sodium borohydride ($NaBH_4$). GO powder and acid-treated MWCNTs were mixed thoroughly with deionized water in a 250 ml beaker in an ultrasonic bath for 30 min. The mixture was then stirred using with a magnetic bar, and a 0.3 M aqueous solution of $NaBH_4$ was slowly added to the GO solution, thereby causing the reduction of GO to GR. The mixture was washed and centrifuged with deionized water a total of six times, and the resulting black powder was then dried in a vacuum at room

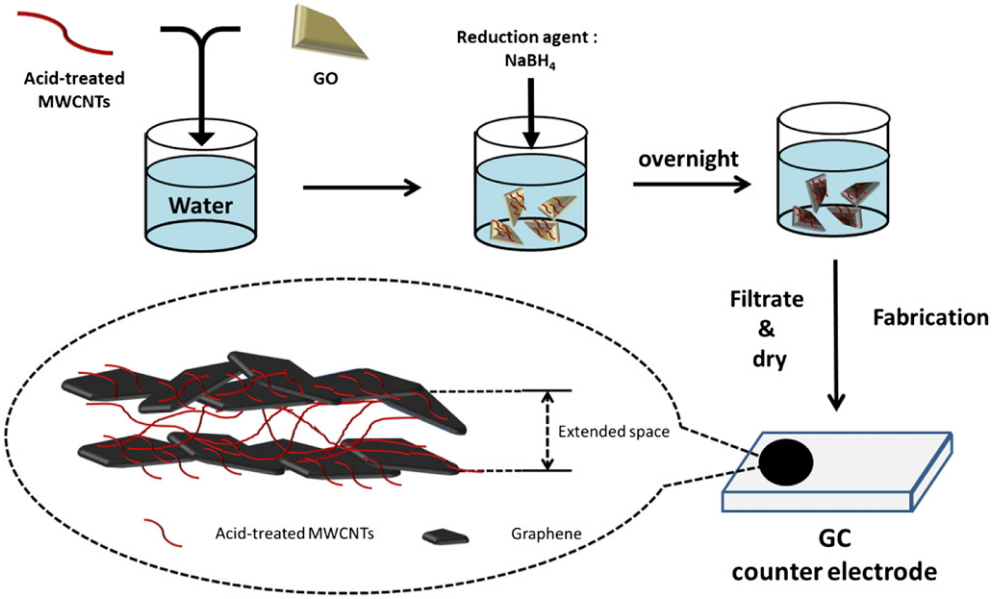

Fig. 1. Illustration of the process used to fabricate the GC counter electrode on FTO.

temperature. Finally, the GC hybrid was formed. GR was also obtained using the same method. The acid treatment of MWCNTs was performed using a nitric acid washing procedure; raw MWCNTs were boiled in concentrated nitric acid for 4 h. The MWCNTs were then filtered, washed with deionized water several times to remove the residual acid, and dried in an oven at 105 °C. The GC hybrids were designated according to the ratio of GR to MWCNTs. The GC hybrid with 30 wt% GR and 70 wt% MWCNTs is hereafter termed GC37; the GC hybrid with 70 wt% GR and 30 wt% MWCNTs is hereafter GC73. All carbonaceous materials were through heat-treatment in an oven at 350 °C. The loading amount of carbonaceous material on a counter electrode is about 4 mg cm^{-2}.

2.2. Preparation of various counter electrodes and fabrication of DSSCs

Platinized counter electrodes, each with a thickness of 50 nm, were prepared using an E-gun evaporator (VTI-940503, Vactech), which was equipped with an oscillating quartz thickness controller (CRTM-5000, Ulvac) to monitor the thickness of the platinum films on the FTO glass. The paste containing GR and GC was fabricated as follows. Firstly, 85 wt% carbon materials, 10 wt% polyvinylidene fluoride (PVDF), and 5 wt% XC-72 were mixed in N-methyl-2-pyrrolidone (NMP) using an ultrasonic horn for 1 h to produce the carbon paste. The carbonaceous counter electrode was fabricated using solvent-casting in a vacuum at 120 °C overnight. In order to prepare the working electrode of the DSSC, a layer of paste was coated on fluorine-doped tin oxide glass (*TEC-7*, 7 Ω $square^{-1}$, *Hartford Glass Co*., USA) plates. The coated electrodes were heated in air at 500 °C for 30 min. The thickness and active cell area of the TiO_2 film were about 10 μm and 0.16 cm^2, respectively. Prior to the fabrication of the DSSCs, the working electrodes were sensitized by soaking them for 24 h in a 3×10^{-4} M solution of ruthenium dye (cis-dithiocyanato-N,N′-bis(2,2′-bipyridyl-4-carboxylicacid-4′-tetra-butylammonium carboxylate) ruthenium (II); N719, Solaronix SA, Switzerland) in acetonitrile/*t*-butyl alcohol (*v*:*v*=1:1). The sensitized electrodes were then immersed in acetonitrile for 12 h. The DSSC was comprised of a sensitized working electrode, various counter electrodes and an electrolyte with a 60 μm thick hot-melt sealing foil (SX1170-60, Solaronix SA, Switzerland) between each layer. The electrolyte used in this study consisted of 0.6 M 1-butyl-3-methylimidazolium iodide (BMII), 0.1 M guanidinium thiocyanate, 0.03 M iodine, and 0.5 M 4-tert-butylpyridine (TBP) in acetonitrile/valeronitrile (volume ratio: 85:15) [23].

2.3. Characterization of carbonaceous counter electrodes

The photocurrent–voltage characteristics of the electrodes were measured using a 2400 digital source meter (Keithley, USA) under illumination by a Class A sunlight simulator of 100 mW cm^{-2} (91160A, AM 1.5, Oriel, Newport Corporation, USA), which was equipped with an AM 1.5G filter (81088A, Oriel, Newport Corporation, USA) and a 300 W xenon lamp (6258, Oriel, Newport Corporation, USA). The intensity of the simulated incident light was calibrated up to 100 mW cm^{-2} using a reference Si solar cell, which was calibrated at NREL (USA). Cyclic voltammetric measurements were carried out using a potentiostat/galvanostat (PGSTAT 302N, Autolab, EcoChemie, Netherlands) in a three-electrode configuration. Platinum wire and an Ag/AgCl electrode were used as the counter and reference electrodes, respectively. Electrochemical impedance spectra (EIS) were obtained using the potentiostat/galvanostat equipped with a Frequency Response Analysis (FRA) module by using symmetrical device in the dark. The frequencies used in the scan ranged from 10^6 to 10^{-1} Hz, and an applied voltage of 10 mV was used. Impedance spectra were analyzed using an equivalent circuit model with Autolab FRA software (v4.9, Eco Chemie B.V.). Raman spectra were recorded using a LabRam I confocal Raman spectrometer (Dilor, France). The excitation wavelength was 488 nm from a He–Ne laser with a laser power of ca. 15 mW at the surface of the sample. The morphology of the carbonaceous counter electrodes was then studied using scanning electron microscopy (SEM, Hitachi S-4700I, Japan), and the microstructures of the carbon materials were also investigated using transmission electron microscopy (TEM, JEOL 2100F, Japan) at an accelerating voltage of 200 kV.

3. Results and discussion

3.1. Analysis of DSSC performance using various counter electrodes

The cell performance of the DSSCs was measured under illumination (1 Sun AM 1.5). Fig. 2 and Table 1 show the characteristics of the DSSCs fabricated using various different counter electrodes. Under illumination, the DSSC with the GR counter electrode exhibited a short-circuit photocurrent (J_{sc}) of 11.95 mA cm^{-2}, an open-circuit voltage (V_{oc}) of 0.78 V and a fill factor (*FF*) of 0.42, yielding a conversion efficiency (η) of 3.90%. For the DSSC with the MWCNTs counter electrode fabricated using exactly the same method, the values of J_{sc}, V_{oc}, *FF* and η were 9.12 mA cm^{-2}, 0.77 V, 0.53 and 3.73%, respectively. The results for the GR and MWCNTs counter electrode show that the improved V_{oc} is a result of the decrease in the Fermi level of the redox species [12,24]. The obvious decrease in FF of the GR and MWCNT counter electrodes maybe attributed to the high electrical resistance of the FTO at the surface of the carbonaceous materials in contact with the electrolyte. According to the structures concerned, the contact area of the GR was probably greater than that of the MWCNTs. Nevertheless, the chemically-reduced GR possesses many isolated aromatic domains, which suppresses the electrical conduction on the basal plane of the GR. One further reason for the lower *FF* value of the GR counter electrode is the higher diffusion resistance. Compared with the platinum film electrode, the MWCNTs electrode has a low *FF*, which results from the small contact area between each CNT, leading to a high internal resistance. Due to its high specific surface area, the GR counter electrode had a higher current density than the CNTs or the platinum film electrode. This result also shows that the concentration of defects on the surface of the GR was higher than that on the MWCNTs. Compared to GR electrodes; the GC hybrid

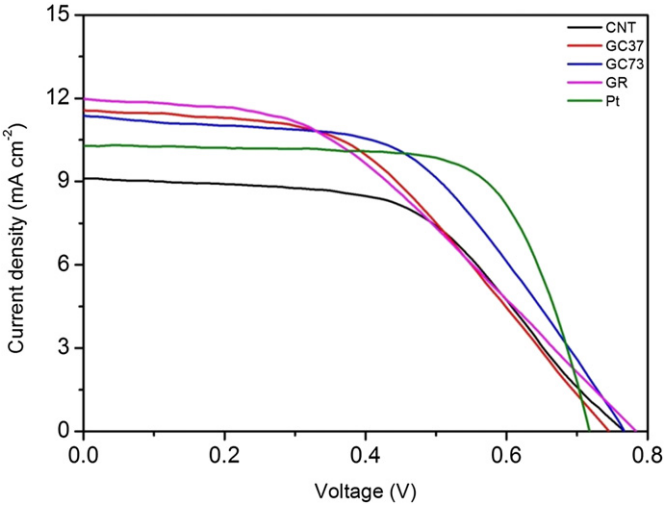

Fig. 2. Photocurrent density-voltage characteristics of the DSSC fabricated using platinum films, GR, GC73, GC37 and CNT counter electrodes.

Table 1
Characteristics of the *J–V* curves of DSSCs with various counter electrodes.

Electrode	J_{sc} (mA cm^{-2})	V_{oc} (V)	*FF*	η (%)
Platinum films	10.26 ± 0.3	0.72 ± 0.01	0.70 ± 0.01	5.09 ± 0.07
GR	11.95 ± 0.5	0.78 ± 0.02	0.42 ± 0.06	3.90 ± 0.49
GC37	11.52 ± 0.4	0.74 ± 0.03	0.47 ± 0.03	3.94 ± 0.12
GC73	11.42 ± 0.2	0.77 ± 0.02	0.53 ± 0.10	4.66 ± 0.29
CNT	9.12 ± 0.3	0.77 ± 0.02	0.53 ± 0.02	3.73 ± 0.36

shows a comparable current density and an enhanced *FF*, with a resulting improvement in cell performance. This indicates that the incorporation of CNTs into GR can effectively be used to rebuild the structure of the carbonaceous materials, and the active sites were also enhanced. There may also be an effect due to the connection of the isolated aromatic domains, thereby affording an improved conductivity to the GR. In addition, due to the effective network of the GC hybrid, the diffusion resistance of the redox species is reduced as a result of its loose structure, which decreases its internal resistance. However, the cell performances of the DSSCs that used the GC37 counter electrode was characterized by a lower *FF* than those that used the MWCNT electrode, suggesting that the GC hybrid with a low GR loading had a higher internal resistance due to the aggregation of the MWCNTs. This increases the charge recombination and results in a lower V_{oc}, which may be attributed to the occurrence of a high dark current. In contrast, the GC73 counter electrode showed a markedly better performance than the platinized FTO; the values of J_{sc}, V_{oc}, *FF* and η were 11.42 mA cm^{-2}, 0.77 V, 0.53, and 4.66%, respectively. The lower *FF* of GC37 may be due to the high loading of MWCNTs. At high MWCNT loadings, the MWCNTs tend to form a bundle, and the GR is attracted to similar "isolated" pads in the MWCNTs bundles, thereby causing significant aggregation. However, this is accompanied by a high diffusion resistance and a high internal resistance, leading to a low V_{oc} due to the increased charge recombination. At high GR loadings of the GC hybrid, the MWCNTs appeared to separate evenly on the surface of the GR due to their interaction with the aromatic domain on the basal plane of the GR. The attached MWCNTs formed a steric barrier that hindered the interaction of the GR sheet with the other sheets, thereby preventing aggregation. For this reason, the structure of the GC73 electrode may be seen to be looser and rougher than that of the GC37. According to these encouraging results of the performance of the GC hybrid as a counter electrode of DSSCs, our next step was to investigate the electrochemical properties of the various carbonaceous counter electrodes.

3.2. Analysis of the electronic structure and electrochemical properties of platinum film, GR, CNT, and GC hybrid electrodes

Raman spectroscopy is a useful tool for investigating the structural variations that occur in carbonaceous materials because it shows both the D band and the G band [25]. Fig. 3 shows the position of the various peaks of the two bands and the in the D/G ratios for the five different carbonaceous materials of interest. An increase in the D/G ratio is generally the result of (a) an increase in the amount of amorphous carbon, (b) a higher defect density, or (c) a decrease in the crystalline size [15]. In our case, the increase in the D/G ratio of the chemically-reduced GR may be due to the high density of the defects on the surface of the GR. However, in the GC hybrid, the low D/G ratio was also influenced by the incorporation of MWCNTs. Due to the connection between the MWCNTs, the isolated aromatic domain on the surface of the GR may cause an increase in the extension of the delocalized π-electrons. In addition, the conductivity of the basal plane on the surface of the GR may be increased. According to the behavior of the catalyst in the counter electrode, the richness of the defects can improve the exchange

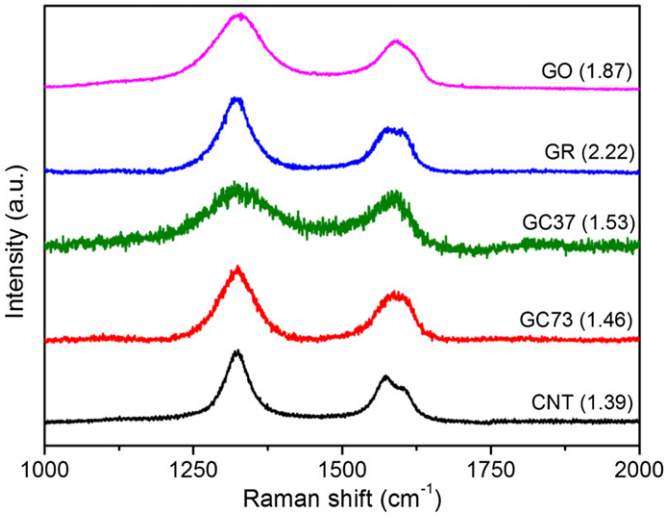

Fig. 3. Raman spectra of GO, GR, GC37, GC73, and CNT with the corresponding D/G ratios.

current density, electroactivity, and electrochemical resistance at the interface. In our next step, we used these materials to investigate the electrochemical properties of electrolytes containing Fe^{2+}/Fe^{3+} and I^-/I_3^-.

Cyclic voltammetry (CV) is a powerful and efficient method of analyzing the catalytic mechanisms that take place in an electrochemical system. We used two types of electrolyte, namely (1) a single electron transfer medium (Fe^{2+}/Fe^{3+}) and (2) a two-electron transfer medium (I^-/I_3^-), in order to investigate the electrocatalytic properties of the carbonaceous materials of interest to us here.

Fig. 4(a) shows the CV results obtained from platinum film, GR, MWCNTs, and the GC hybrids in aqueous solutions containing 6 mM $K_3Fe(CN)_6$ and 1 M KNO_3. According to the literature [26,27], the peak separation (ΔE_p) is related to the electron transfer rate, with a higher electron transfer rate (k) being associated with lower value of ΔE_p. ΔE_p is 158 mV for platinum films and 109 mV for GR, indicating that the electron transfer rate of GR is higher than that of platinum film, which may be attributed to the higher concentration of defects and the greater hydrophilicity of the oxygen-containing GR. In addition, the exchange current density of GR is higher than that of the platinum film due to its greater specific surface area. Furthermore, the electron transfer rates and exchange current densities of the GC hybrids (GC37 and GC73) are higher than those of the other materials due to their low ΔE_p values (85 and 83 mV, respectively). In contrast to platinum film and the GR electrode, the GC hybrids possess higher specific surface areas and hydrophilicities, and therefore show impressive electrocatalytic properties, due to the incorporation of MWCNTs. In addition, the change in internal spacing of the GR due to the incorporation of the MWCNTs resulted in improvements to the effectiveness of the active sites on the surface. In order to simulate the conditions of the redox reaction of the iodide ions at the counter electrode of the DSSC, we used a solution containing iodide/triiodide to perform the CV measurements, as shown in Fig. 4(b). For the platinized FTO electrode, two groups of redox peaks can be seen. The middle peaks may be attributed to Eq. (1) and the peaks on the right may be assigned to Eq. (2) [12,24,28]. The peaks on the left are probably partially caused by the moisture present in the carbon materials.

$$3I^- \leftrightarrow I_3^- + 2e^- \quad (1)$$

$$2I_3^- \leftrightarrow 3I_2 + 2e^- \quad (2)$$

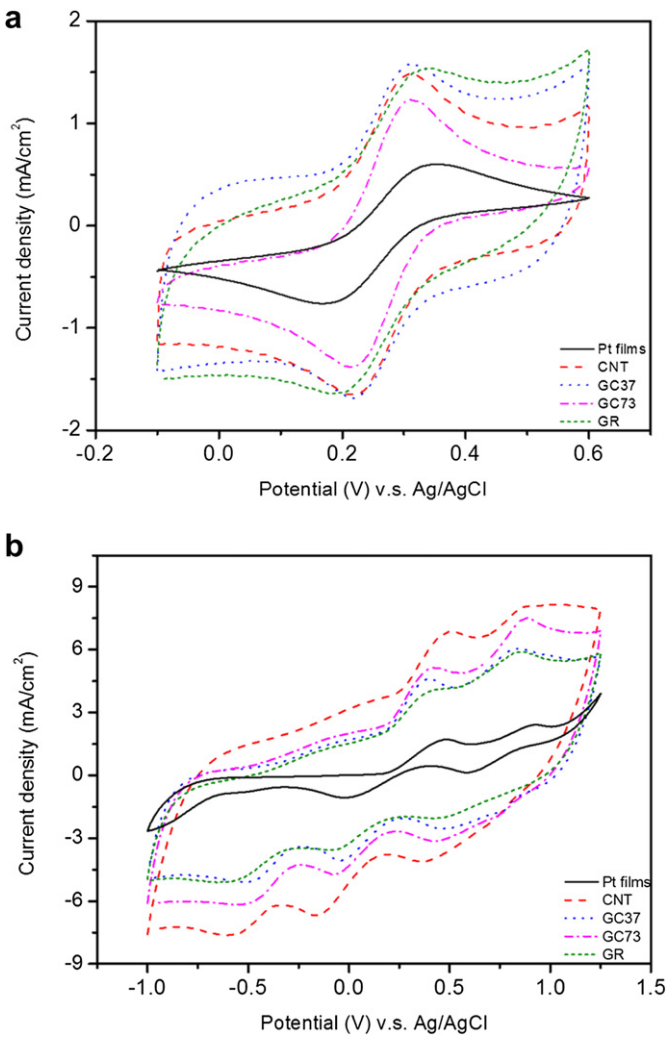

Fig. 4. Cyclic voltammograms of platinum films, GR, CNT, and the GC electrode at a scan rate of 50 mV s^{-1} in (a) 6 mM $K_3Fe(CN)_6$ aqueous solution containing 1 M KNO_3 and (b) 10 mM LiI, 1 mM I_2 acetonitrile solution containing 0.1 M $LiClO_4$.

The CV results for the GR and GC hybrid electrodes show that, these carbon electrodes exhibit a high current density in the middle peaks due to their high specific surface area. In addition, the GC hybrid electrode exhibited a higher current density than the GR electrodes due to improvements to the effective specific surface area and their active site reaction. The incorporation of MWCNTs into the space between the GR sheets may suppress strong π–π interaction, causing an increased reaction at the active sites. Hence, the exchange current density on the surface of the GR was improved. Interestingly, the right-hand peaks of the GC73 electrode that were attributed to Eq. (2) showed a similar current density to that of the GR electrode, implying that the reaction of Eq. (2) was maintained even in the presence of the MWCNTs. Although the MWCNTs exhibited the highest exchange current density, the electron transfer rate was poor, compared with the other carbon electrodes (GR and GC hybrid). It appears that MWCNTs maybe an unsuitable material for the counter electrode. In addition, compared with GR (416 mV) and MWCNTs (598 mV), somewhat similar ΔE_p values may be seen in the middle peaks of GC37 (403 mV) and GC73 (435 mV), indicating that the electroactive properties of GR were maintained, even when the MWCNTs with a low electron transfer rate were incorporated. The GC hybrid possessed both a high electron transfer rate and a high exchange current density contributed to the GR and the MWCNTs. In addition, the MWCNTs were introduced to the GR in order to increase the space between the GR sheets, and it may be that they therefore assist in the diffusion of the redox ions in the catalyst. The CV results show that the use of a carbonaceous material as a counter electrode in a DSSC affords it a comparable improvement in its properties compared to those of DSSCs that use a platinized FTO, due to the remarkable electrocatalytic properties of the carbonaceous materials. In order to investigate the operation of a real DSSC device, we next used electrochemical impedance spectra to characterize the charge transfer behavior and diffusion resistance.

Electrochemical impedance spectroscopy (EIS) has been used recently to analyze the kinetic behavior of counter electrodes in DSSCs [15–17]. In general, the impedance spectra of counter electrodes of DSSCs form two semicircles that represent the two different steps of the reaction that occurs in the electrochemical process, namely the charge transfer at the platinum/electrolyte interface, and the diffusion of I^-/I_3^- ions in the electrolyte. The charge transfer resistance (R_{CT}) may be correlated with the exchange current density (J_0), while the triiodide is reduced to iodide at the counter electrode [15,17]. The exchange current density is calculated from the charge transfer resistance using Eq. (3) [29]:

$$J_0 = \frac{RT}{nFR_{CT}} \tag{3}$$

where R, T, n, and F represent the gas constant, the temperature, the numbers of electrons transferred in the reduction reaction, and the Faraday constant, respectively.

The Nyquist plots of various symmetrical devices fabricated using carbonaceous electrodes are shown in Fig. 5(a), which also shows the equivalent circuit used to fit the EIS spectra. The semicircle on the left (at high frequency) corresponds to the charge transfer process, and the semicircle on the right (at low frequency) may be attributed to the diffusion of iodide/triiodide in the electrolyte. The charge transfer resistance of GR is lower than that of platinum film. This finding implies that the charge transfer process at the surface of GR is faster than it is for platinum film as a result of the higher exchange current density, in agreement with the CV results. Due to the high concentration of defects and the electrical conductivity, the charge transfer behavior of chemically-reduced GR was improved, indicating its potential as an alternative to the platinum catalyst. However, the diffusion resistance of the GR electrode was significantly higher than that of the platinum films, indicating that the microstructure of the GR electrode suppresses the diffusivity of the redox species [16]. Due to the high degree of π–π interaction between the GR sheets, GR may be seen to have a stacked morphology that is characterized by a significant degree of aggregation, which leads to the formation of small pores in the GR electrode. In contrast to GR, the GC hybrid electrode showed a smaller charge transfer resistance and a remarkable resistance to diffusion. Because MWCNTs were incorporated into the sheets of the GR, the dispersive ability of the GR sheets was improved [22,30], and furthermore the redox ions could easily be transferred within the hybrid sheets due to the increased space within the GR. Hence, the diffusion resistance of the GC hybrid was decreased. The low charge transfer resistance caused the device to respond more quickly due to its improved electrocatalytic properties and electrical conductivity, implying an improved reduction ability for iodide/triiodide. According to the results of the Nyquist plot, the charge transfer resistance of the GC73 was lower than that of the GC37, consistent with the CV results. However, there is still a weak correlation between the charge transfer rate and the cell performance. Hence, because of the working principle of the counter electrode, in which electrons are transferred from the outside

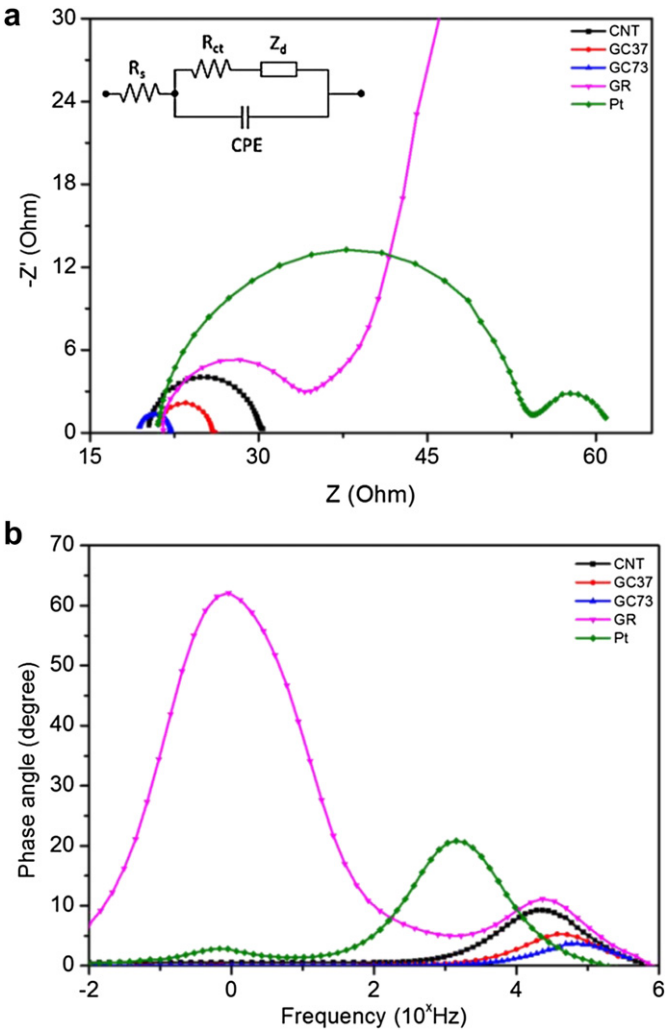

Fig. 5. (a) Nyquist plot of symmetrical cells for frequencies in the range 10^6–10^{-2} Hz. The insets show the equivalent circuit of the device (b) Bode plot of symmetrical cells with various carbon-based electrodes.

circuit to the catalyst, the electrons are transferred through the catalyst to the interface between the catalyst and the electrolyte. There are therefore three interfaces, namely (1) the interface between the FTO and the catalyst, (2) the conductive path of the catalyst, and (3) the interface between the catalyst and the electrolyte. In the Bode plot, both the conductive path and the lifetime of the electrons in the catalyst should be considered. Choi et al. discussed the correlation between charge transfer rate and frequency, and showed that a higher frequency indicated a higher charge transfer rate [18]. The Bode plots of various symmetrical devices fabricated using carbonaceous electrodes are shown in Fig. 5(b), which shows the electrochemical response of the interface in the device at various frequencies. According to the Nyquist plot, charge transfer behavior was observed at high frequency (right-hand peak); diffusion behavior was observed at low frequency (left-hand peak). Fig. 5(b) shows that the platinized FTO had a response log frequency at 3.153, indicating the long lifetime of the electrons. Compared to platinized FTO, the GR and MWCNTs showed a higher response frequency, implying a similar but lower electron lifetime. Here, the microstructure of the carbon electrode should be considered. In this case, the GR showed a stacking morphology due to the strong interactions, which increased the resistance for the hopping of electrons between GR sheets. Although MWCNTs have a high aspect ratio, the considerable aggregation of MWCNTs may increase the lifetime of the electrons, and may decrease the electron transfer rate. Recombination may occur, thereby decreasing the performance. The GC hybrid shows a low electron lifetime. Due to the incorporation of MWCNTs into the GR, the conductivity between the GR sheets may be improved and the isolated aromatic domains on the GR may also be connected to extend the delocalized domain of the electrons, thereby enhancing the conductivity of the GR. Furthermore, the GC73 exhibited the highest frequency, implying the lowest electron lifetime. Due to the incorporation of MWCNTs, the connections between the GR sheets were improved, potentially improving the internal resistance of the GR. On other hand, the structure of GC73 contained a low ratio of MWCNTs, thereby decreasing the formation of CNT bundles. Effective conducting paths may be formed in the GR sheets. In contrast to GC73, GC37 has a higher ratio of MWCNTs, trapping the transferring electrons in the MWCNTs. Hence, the response frequency of GC37 was higher than that of GC73, implying a high electron lifetime. Furthermore, the value of the series resistance was similar to that of the other electrodes. The EIS results are summarized in Table 2. The results of Raman spectra, CV, and EIS spectra show that the GC electrode possessed the most favorable electrocatalytic properties for use as a potential catalytic alternative to platinum film, showing that it should be possible to replace the platinum with this material in counter electrodes.

3.3. Analysis of the morphology of GR, CNT, and GC hybrid electrodes

Fig. 6 shows TEM images of the microstructures of various carbonaceous materials consisting of various ratios of MWCNTs to GR. Fig. 6(a) shows that the morphology of GR is characterized by a rough wrinkled and aggregated surface, which may be attributed to the stacking of several different pieces of GR due to the strong π–π staking interaction at its the surface. Fig. 6(b) shows the morphology of GC37. Excess MWCNTs were not individually adsorbed to the surface, but rather formed bundles or clusters with a self-aggregated morphology [31]. In contrast, GC73 (Fig. 6(c)) shows that the individual MWCNTs appeared to be evenly separated on the surface of the GR due to the interaction with the π-conjugated aromatic domain on the basal plane of the GR. The attached MWCNTs formed a steric barrier that hindered the interaction of the GR sheet with the other sheets, thereby preventing aggregation. According to the TEM results, the GC hybrid showed a morphology in which MWCNTs were attached to the surface of the GR. These results show that the attached MWCNTs may not only enhance the conductivity of the GR at the surface, but may also improve the electron transfer between the GR sheets due to the connection of the isolated aromatic domains. In addition, the MWCNTs attached to the GC73 showed a high degree of dispersion. This may constitute a more efficient conductive path for electrons, thereby improving the electron transfer rate of the GC hybrid catalyst. According to the results of CV and EIS, carbonaceous materials exhibit remarkable properties in terms of electroactivity

Table 2
Series resistance (R_s), charge transfer resistance (R_{CT}), and diffusion resistance (R_d) of the DSSCs fabricated using various carbonaceous electrodes.

Electrode	R_s (Ω cm^2)	R_{CT} (Ω cm^2)	log (frequency)
CNT	19.68	13.97	4.367
GC37	20.96	4.95	4.571
GC73	19.30	2.94	4.857
GR	21.53	14.23	4.367
Platinum films	20.90	33.1	3.153

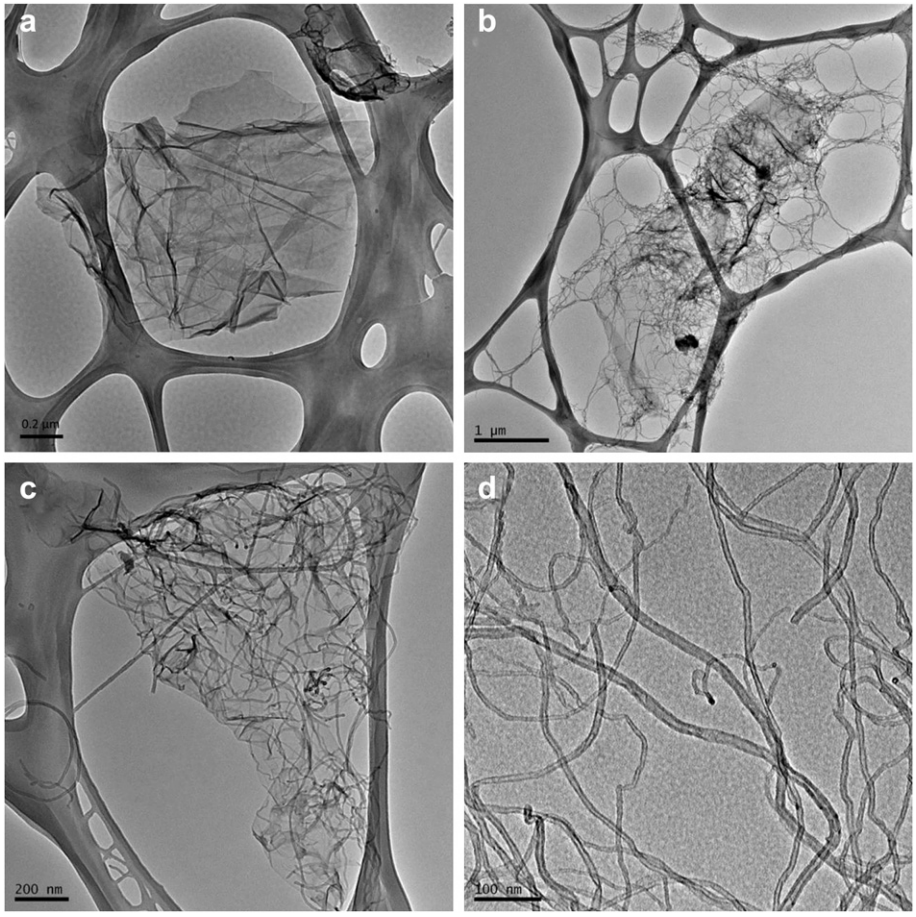

Fig. 6. TEM images showing the morphology of (a) GR, (b) GC37, (c) GC73, and (d) CNT.

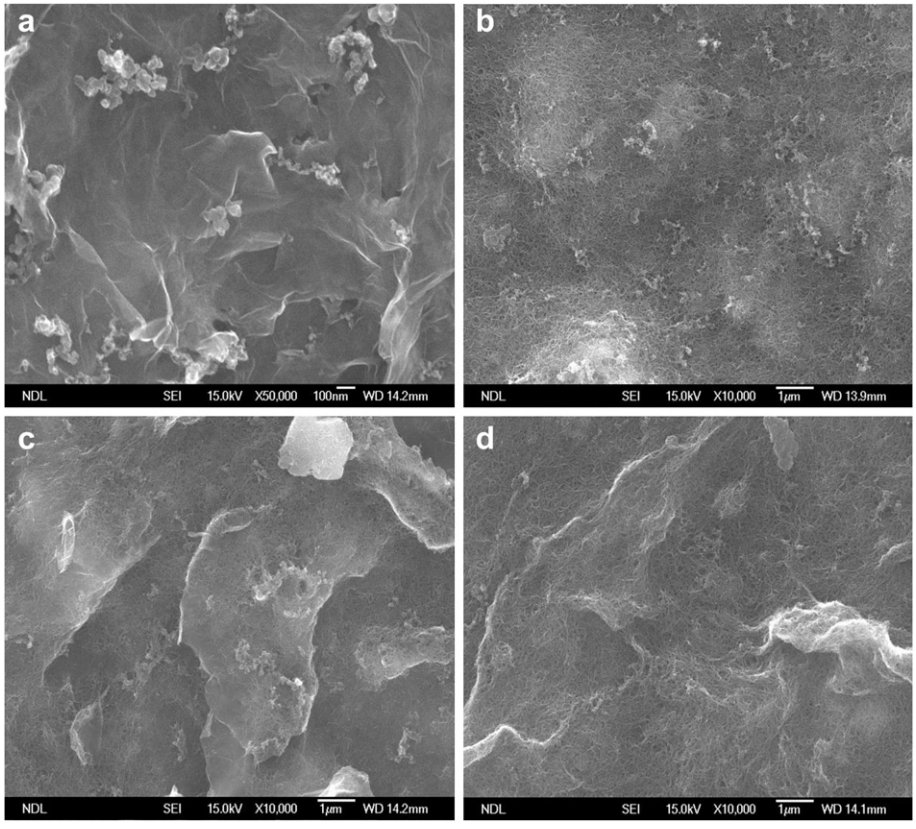

Fig. 7. SEM images showing the morphology of the counter electrode fabricated using (a) GR, (b) GC37, (c) GC73, and (d) CNT.

and exchange current density, especially in terms of diffusion resistance and electron lifetime. In order to provide clearer evidence, we next used the SEM to observe the morphology of the carbon electrode.

Fig. 7 shows the morphology of the carbon electrodes, and provides some evidence to explain the differences in their diffusion resistance and microstructure. Due to the strength of the π–π interaction within the GR, its morphology may be seen to be a stacked surface with small pores, which indicates that I^- may not easily be transferred through the limited channels of the microstructure, thereby increasing the internal resistance of the counter electrode, even though GR has a higher rate of charge transfer. In comparison with GR, the GC37 electrode showed a smooth surface. Due to the strong interaction between the CNTs, the dispersed behavior of the GR is similar to an isolated conductive pad in a tangle of conductive wires. However, the GC73 had morphology with a high roughness. The GR in the GC73 showed its function as a conductive pad, and the MWCNTs acted as a wire to connect each GR pad, thereby enhancing the conductivity. In addition, compared with the GC37, the morphology of the GC73 shows a greater amount of space that allows the redox species to diffuse easily. Due to the incorporation of the CNTs into the GR, the space between the GR sheets was increased, thereby decreasing the diffusion resistance of the GC73 counter electrode. All the foregoing results showed consistency within the TEM, SEM, CV and EIS measurements, and showed that the GC73 electrode possesses the most favorable electrocatalytic properties for use as a potential catalytic alternative material to platinum film, thereby reducing the need for platinum in counter electrodes.

The incorporation of GC73 has been shown to increase the charge transfer rate, and to decrease the internal resistance as a result of its electrocatalytic properties that help to decrease the diffusion resistance, and decrease the electron lifetime in hybrid counter electrodes. The use of GC73 hybrid counter electrodes in DSSCs clearly meets the aim of replacing platinum as a key material in DSSCs.

4. Conclusions

We have herein described a GC hybrid material that can be used as an alternative to platinized FTO in DSSC counter electrodes. Results obtained from Raman spectra confirmed the hypothesis that the introduction of the MWCNTs can yield improvements in the electronic structure of GR, due to the connection of the isolated aromatic domains on the surface of GR. Furthermore, CV and EIS results showed that the incorporation of CNTs into GR sheets improved both the electrocatalytic properties and the exchange current density, thereby achieving a satisfactory electron transfer rate at the interface. The results of a Bode plot showed that the incorporation of MWCNTs into GR afforded a connection between the GR sheets and decrease the electron lifetime, therefore improving the electron transfer rate. The cell performances of DSSCs that used a GC counter electrode reached 91.6% of those prepared using a platinized FTO electrode. This was the result of an increased charge transfer rate, a reduced internal resistance, and a decreased electron lifetime produced by the incorporation of the GC material. Our findings show that graphene/MWCNTs hybrid materials have great potential for DSSC-related applications, and merit further investigation.

References

[1] M. Gratzel, Nature 414 (2001) 338–344.
[2] B. O'Regan, M. Gratzel, Nature 353 (1991) 737–740.
[3] T.N. Murakami, S. Ito, Q. Wang, M.K. Nazeeruddin, T. Bessho, I. Cesar, P. Liska, R. Humphry-Baker, P. Comte, P. Pechy, M. Gratzel, J. Electrochem. Soc. 153 (2006) A2255–A2261.
[4] J. Chen, K. Li, Y. Luo, X. Guo, D. Li, M. Deng, S. Huang, Q. Meng, Carbon 47 (2009) 2704–2708.
[5] K.-M. Lee, C.-W. Hu, H.-W. Chen, K.-C. Ho, Sol. Energy Mater. Sol. Cells 92 (2008) 1628–1633.
[6] G. Calogero, F. Bonaccorso, O.M. Marago, P.G. Gucciardi, G. Di Marco, Dalton Trans. 39 (2010) 2903–2909.
[7] J. Li, A. Cassell, L. Delzeit, J. Han, M. Meyyappan, J. Phys. Chem. B 106 (2002) 9299–9305.
[8] J. Han, H. Kim, D.Y. Kim, S.M. Jo, S.-Y. Jang, ACS Nano 4 (2010) 3503–3509.
[9] W.J. Lee, E. Ramasamy, D.Y. Lee, J.S. Song, ACS Appl. Mater. Inter. 1 (2009) 1145–1149.
[10] J.E. Trancik, S.C. Barton, J. Hone, Nano Lett. 8 (2008) 982–987.
[11] S.H. Seo, S.Y. Kim, B.-K. Koo, S.-I. Cha, D.Y. Lee, Langmuir 26 (2010) 10341–10346.
[12] K. Imoto, K. Takahashi, T. Yamaguchi, T. Komura, J.-i. Nakamura, K. Murata, Sol. Energy Mater. Sol. C 79 (2003) 459–469.
[13] G. Veerappan, K. Bojan, S.-W. Rhee, ACS Appl. Mater. Inter. 3 (2011) 857–862.
[14] Y. Xu, H. Bai, G. Lu, C. Li, G. Shi, J. Am. Chem. Soc. 130 (2008) 5856–5857.
[15] P. Hasin, M.A. Alpuche-Aviles, Y. Wu, J. Phys. Chem. C 114 (2010) 15857–15861.
[16] J.D. Roy-Mayhew, D.J. Bozym, C. Punckt, I.A. Aksay, ACS Nano 4 (2010) 6203–6211.
[17] L. Kavan, J.H. Yum, M. Gratzel, ACS Nano 5 (2010) 165–172.
[18] H. Choi, H. Kim, S. Hwang, Y. Han, M. Jeon, J. Mater. Chem. 21 (2011) 7548–7551.
[19] M.-Y. Yen, C.-C. Teng, M.-C. Hsiao, P.-I. Liu, W.-P. Chuang, C.-C.M. Ma, C.-K. Hsieh, M.-C. Tsai, C.-H. Tsai, J. Mater. Chem. 21 (2011) 12880–12888.
[20] H. Choi, H. Kim, S. Hwang, W. Choi, M. Jeon, Sol. Energy Mater. Sol. Cells 95 (2011) 323–325.
[21] G. Zhu, L. Pan, T. Lu, T. Xu, Z. Sun, J. Mater. Chem. 21 (2011) 14869–14875.
[22] M.-Y. Yen, M.-C. Hsiao, S.-H. Liao, P.-I. Liu, H.-M. Tsai, C.-C.M. Ma, N.-W. Pu, M.-D. Ger, Carbon 49 (2011) 3597–3606.
[23] S. Ito, T.N. Murakami, P. Comte, P. Liska, C. Grätzel, M.K. Nazeeruddin, M. Grätzel, Thin Solid Films 516 (2008) 4613–4619.
[24] P. Li, J. Wu, J. Lin, M. Huang, Y. Huang, Q. Li, Sol. Energy 83 (2009) 845–849.
[25] A.C. Ferrari, J. Robertson, Phys. Rev. B 61 (2000) 14095.
[26] E. Ramasamy, J. Lee, Carbon 48 (2010) 3715–3720.
[27] R.S. Nicholson, Anal. Chem. 37 (1965) 1351–1355.
[28] Z. Huang, X. Liu, K. Li, D. Li, Y. Luo, H. Li, W. Song, L. Chen, Q. Meng, Electrochem. Commun. 9 (2007) 596–598.
[29] A.J. Bard, L.R. Faulkner, Electrochemical Methods: Fundamentals and Applications, second ed., Wiley, New York, 2001.
[30] C. Xu, X. Wang, J. Zhu, J. Phys. Chem. C 112 (2008) 19841–19845.
[31] C. Zhang, L. Ren, X. Wang, T. Liu, J. Phys, Chem. C 114 (2010) 11435–11440.